Inorganic Chemistry

Open Access
This article is licensed under CC-BY 4.0

pubs.acs.org/IC
Article

Enhanced Ion-Exchange Properties of a Complex Microporous Uranyl Borophosphate

Yucheng Hao,* Xu Jingli, Thomas E. Albrecht, Shuao Wang, Rüdiger-A. Eichel, and Evgeny V. Alekseev*

Cite This: *Inorg. Chem.* 2025, 64, 24754−24765

Read Online

ACCESS | Metrics & More | Article Recommendations | Supporting Information

ABSTRACT: An unusual microporous uranyl borophosphate has been prepared under mild hydrothermal conditions, namely, $Cs_3(UO_2)_3[B(PO_4)_4](H_2O)_{0.5}$ denoted as CUPB1. It crystallizes in the chiral space group $P4_12_12$. The three-dimensional (3D) open framework of CUPB1 is constructed by $[B(PO_4)_4]^{9-}$ fundamental building blocks (FBBs) linked by UO_7 pentagonal bipyramids into nanoscale size (~12.2 Å × 12.2 Å × 11.7 Å) uranyl borophosphate cages of $U_{12}P_{24}B_8$. The Cs^+ cations are disordered and are located near the cage windows. Free void volume in CUPB1 is ~59% based on the single-crystal X-ray diffraction data, which makes it a highly porous compound. Moreover, the porosity and flexibility of the Cs^+ cations in the framework make it exchangeable with most monovalent and divalent cations in aqueous solutions. We have studied the ion-exchange properties in detail with the environmentally relevant cations Pb^{2+}, Co^{2+}, and Ni^{2+}, as well as the key nuclear fission products Sr^{2+} and Ba^{2+}, at both room temperature and ~70 °C. The simple synthetic route, microporous structure, thermal stability, vibrational spectroscopy, and ion-exchange properties are discussed in detail.

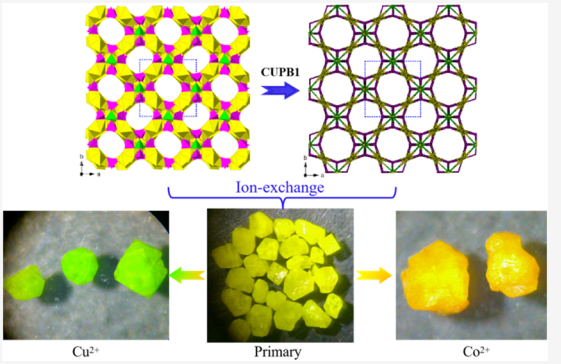

1. INTRODUCTION

Open framework materials are of high interest field due to their fascinating structures and important applications.[1] They can be used in areas as diverse as ion exchangers, gas adsorption and storage, catalysts, nonlinear optical materials, etc.[2] zeolites[3a] and metal−organic framework[3b] (MOF) materials are typical examples, which always possess highly porous framework structures. Zeolites are characterized as the oxo-tetrahedral framework structures, such as aluminosilicates,[4a] aluminogermanates,[4b] aluminophosphates,[4c] and zinc phosphates.[4d] MOFs are defined as compounds consisting of metal ions or clusters coordinated to organic ligands to form three-dimensional (3D) framework structures.[3b] However, the thermal stabilities and expenses of MOFs have limited the vast applications in the industry.[5,6]

The substitution of boron for aluminum/silicon in zeolites has long been a topic of interest, because the resulting oxoborates have complex structural chemistry and remarkable properties.[7,8] Borates possess the intrinsic structural complexity, owing to the ability of the B^{3+} ion to occur in triangular BO_3 and tetrahedral BO_4 coordination environments in the same structure.[9] These two basic units via corner or edge sharing polymerized into clusters, chains, scaffolds, and even 3D open framework structures.[10,11] Boralite, $Zn_4O(BO_2)_6$,[12] is a rare example of complete boron substitution for both Si and Al, which is a direct topological analogue of the aluminosilicate sodalite-type framework found in $Na_4OH(AlSiO_4)_3$.[13] The zeolite-like network of $Na_2Co_2B_{12}O_2$[14] is the first infinite borate containing a discernible tunnel structure, in which the Na^+ within the tunnels are mobile, and exchangeable with Li^+ preservation of the original crystal morphology. The actinide borate, $[ThB_5O_6(OH)_6][BO(OH)_2]\cdot 2.5H_2O$ (NDTB-1),[15a] which has a porous super tetrahedral 3D framework structure, possess exceptional ion-exchange properties toward TcO_4^-.[15b,16] The incorporation of those mixed oxo-anions, such as $[SiO_4]^{4-}$, $[AlO_4]^{5-}$, $[GeO_4]^{4-}$, $[PO_4]^{3-}$, etc., gave rise to new families of borates derivative materials.[17,18] From the previously reported results,[17] the introduction of mixed oxo-anions into borates system, the resulting structures are favorite to form higher dimensional 3D open frameworks. For example, borosilicate $Cs_2B_4SiO_9$[19] and its basic B_4O_{10} groups are connected with neighboring SiO_4 tetrahedra forming a 3D network, which is a deep-ultraviolet nonlinear optical crystal. The organic templated aluminoborate, $[CH_3NH_3]_{1.5}[CH_3CH_2CH_2NH_3]_{0.5}[H_2O]_5[Al(B_5O_{10})]$,[20] shows an unprecedented 3D intersecting channel system. The framework is built from the strict alternation of B_5O_{10} clusters and AlO_4 tetrahedra. Borogermanate, $SrGe_2B_2O_8$,[21] has a 3D

Received: September 25, 2025
Revised: October 29, 2025
Accepted: November 18, 2025
Published: December 9, 2025

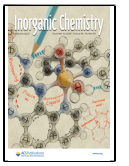

Downloaded via FORSCHUNGZENTRUM JUELICH on January 27, 2026 at 15:24:22 (UTC).
See https://pubs.acs.org/sharingguidelines for options on how to legitimately share published articles.

ACS Publications
© 2025 The Authors. Published by American Chemical Society

https://doi.org/10.1021/acs.inorgchem.5c04481
Inorg. Chem. 2025, 64, 24754−24765

open anionic framework structure, composed of B_2O_7 and Ge_2O_7 dimers with alternate connections. The large B−Ge 8-ring tunnels that hold the Sr^{2+} cations make the Sr^{2+} cations movable at higher temperatures, which has a certain ion-exchange property with the toxic Cd^{2+} cations in the solution.[22]

Borophosphates (BPOs) have been widely studied for their diverse structural architectures and broad applications.[23] Since the first zeolite-like borophosphate $(C_2H_{10}N_2)$-$[CoB_3P_3O_{12}(OH)_{12}]_{18}$ was reported in 1996, a plethora of open framework borophosphates have been prepared under different conditions.[23] The borophosphate frameworks are quite complex and feature various anionic partial structures, such as oligomeric units, 1D chains and ribbons, 2D sheets, and 3D open frameworks.[23] These abundant BPO frameworks were formed from the different templated cations, which are alkali, alkaline earth, transition metal, lanthanide elements, as well as the organic templates.[24,25] Among them, only a few materials own the ion-exchange properties, for example, open framework vanadium borophosphate $Na_2[VB_3P_2O_{12}(OH)]\cdot 2.92H_2O$,[26a] chromium/aluminum borophosphate $Na_8[Cr_4B_{12}P_8O_{45}(OH)_4][P_2O_7]\cdot 8H_2O$,[26b] and aluminum borophosphate $Na_3[Al_2B_6P_4O_{22}(OH)_3](H_2O)_6$.[27] More importantly, the open frameworks of borophosphates are capable of maintaining 5f-elements (actinides) of different oxidation states, as well as providing a stable matrix for interrogating isotopes with short half-lives.[28] To the best of our knowledge, there are quite limited open framework actinide borate phosphates/borophosphates[29] have been reported compared to the actinide-free series. Borate phosphates, such as $U_2(BO_4)(PO_4)$ and $Th_2(BO_4)(PO_4)$, along with borophosphates like $Ag_2(NH_4)_3[(UO_2)_2\{B_3O(PO_4)_4(PO_4H)_2\}]H_2O$, $K_5(UO_2)_2[B_2P_3O_{12}(OH)]_2(OH)(H_2O)_2$, $Pu(H_2O)_3(B_2(OH)$-$(H_2O)(PO_4)_3)$, etc., exhibit remarkable diversity in their structural chemistry.[29,30] The synthesis of novel microporous open framework actinide borate phosphates/borophosphates is a great challenge. Compared to transition metal or lanthanide MOFs, the uranyl cation (UO_2^{2+}) has a series of unique properties: high stability, fixed linear geometry, which directs specific structural motifs, and its relevance to the chemistry of nuclear materials. Unlike many MOFs,[5,6] which can be unstable in water or radiation fields, dense inorganic uranyl compounds reported, for example, by zur Loye group, like $A_2(UO_2)B_2O_5$(A = Cs, Rb, K),[31b] $A_4[(UO_2)_3(PO_4)_2O_2]$(A = alkali metals),[31c] and $Cs_2(UO_2)Al_2O_5$,[31d31d] are often highly resistant to radiation damage and can be stable in aqueous environments, making them more suitable for applications like radioactive waste immobilization or separation.

Herein, the first cesium uranyl borophosphate $Cs_3(UO_2)_3[B(PO_4)_4](H_2O)_{0.5}$(CUPB1) was prepared and reported. It is a microporous material and features a novel 3D open framework structure. An unprecedented spherical uranyl borophosphate cage, $U_{12}P_{24}B_8$, can be observed within its network. The unique structural architecture has been analyzed, together with thermogravimetric and differential scanning calorimetry characterizations, Raman spectroscopy, and exceptional ion-exchange properties are discussed in detail.

2. EXPERIMENTAL SECTION

Caution! The $UO_2(NO_3)_2\cdot 6H_2O$ used in this work contained natural uranium; nevertheless, the standard precautions for handling radioactive materials must be followed.

2.1. Materials and Methods. $UO_2(NO_3)_2\cdot 6H_2O$ (International Bioanalytical Industries, Inc.), H_3PO_3 (Alfa-Aesar, 99.5%), $CsOH\cdot XH_2O$ (X = 15−20%) (Sigma-Aldrich, 99%), and H_3BO_3 (Alfa-Aesar, 99.5%). $NaNO_3$ (Alfa-Aesar, 99.5%), KNO_3 (Alfa-Aesar, 99.5%) $RbNO_3$ (Alfa-Aesar, 99.5%), $Mg(NO_3)_2\cdot 6H_2O$ (Alfa-Aesar, 99.5%), $Ca(NO_3)_2\cdot 4H_2O$ (Alfa-Aesar, 99.5%), $SrCl_2\cdot 6H_2O$ (Alfa-Aesar, 99.5%), $BaCl_2\cdot 2H_2O$ (Alfa-Aesar, 99.5%), $NiCl_2\cdot 6H_2O$ (Alfa-Aesar, 99.5%), $CoCl_2\cdot 6H_2O$ (Alfa-Aesar, 99.5%), $Cu(NO_3)_2\cdot 6H_2O$ (Alfa-Aesar, 99.5%), $Zn(NO_3)_2\cdot 6(H_2O)$ (Alfa-Aesar, 99.5%), $Cd(NO_3)_2\cdot 6H_2O$ (Alfa-Aesar, 99.5%), $PbCl_2$ (Alfa-Aesar, 99.5%), $Bi(NO_3)_3$ (Alfa-Aesar, 99.5%), $[La-Lu(NO_3)_3\cdot 6H_2O]$ (Alfa-Aesar, 99.5%), and $Th(NO_3)_4\cdot 5H_2O$ (International Bioanalytical Industries, Inc.).

2.1.1. Synthesis of CUPB1. Compound CUPB1 was synthesized from the hydrothermal method with initial compositions of $UO_2(NO_3)_2\cdot 6H_2O$ (0.0515 g, 0.10 mmol), $CsOH\cdot xH_2O$ (0.0605 g, 0.40 mmol), H_3PO_3 (0.0332 g, 0.40 mmol), H_3BO_3 (0.0649 g, 1.05 mmol), and deionized water (0.5 mL) with a ratio of U:Cs:P:B = 1:4:4:10. All the chemicals were mixed thoroughly in an agate mortar and then sealed into a Teflon-lined stainless steel autoclave (23 mL). The autoclave was put into a box furnace and heated up to 220 °C for 36 h, and then cooled down to 50 °C at a cooling rate of 3 °C/h. Then, the furnace was switched off. The resulting products were washed with hot water and ethanol to get rid of the excessive boric acid. Yellow large block-shaped crystals CUPB1 together with a greenish byproduct crystals of $Cs_2(UO_2)_2(PO_4)_2$[31] were obtained. The yield of CUPB1 is as high as ca. 49% based on the U content. Pure phases of CUPB1 were obtained from picking up large crystals. The pure phase and ion-exchanged samples of CUPB1 were characterized and confirmed by using laboratory XRD (Figures S1 and S2). Energy-dispersive X-ray spectroscopy (EDS) elemental analyses on the crystals of CUPB1 yield a molar ratio result of U:Cs:P = 3.08:2.96:3.95, which is consistent with the composition obtained from single-crystal diffraction studies (Figure S3).

2.1.2. Ion-Exchange Experiments of CUPB1. Ionic exchange reactions were performed by polycrystalline CUPB1 (50 mg) in scintillation vials with 10 mL of ∼0.005 M $SrCl_2(H_2O)_6$ (aq), $BaCl_2(H_2O)_2$ (aq), $PbCl_2$ (aq), $NiCl_2(H_2O)_6$ (aq), and $CoCl_2(H_2O)_6$ (aq) solutions. The reactions were kept at room temperature for 2 h under magnetic stirring and then transferred into a box furnace at 70 °C for 12 h. The ion-exchanged samples were separated through filtration, washed with excess of water and acetone for 1 day, and then placed into a drying oven for 24 h. The compositions and element distributions of exchanged samples were measured by EDS measurements.

The kinetic studies of Sr^{2+}, Ba^{2+}, Pb^{2+}, Co^{2+}, and Ni^{2+} ion-exchanged by CUPB1 were carried out as follows. Nine parallel solutions (10 mL) for each cation (0.005 M) were mixed with the same ratios of A^{2+}:CUPB1 = 3:2 (A^{2+}:Cs^+ = 1:2, 50 mg CUPB1 sample for each), and the mixtures were kept under magnetic stirring at room temperature (RT). The ion-exchange experiments were performed for nine different reaction times (1.5, 4, 21, 26, 45, 48, 52, 69, and 74 h). For comparison, the second series of experiments were performed in a box furnace at 70 °C with the same reaction times. The suspensions were filtered at certain reaction times, and the filtrates were analyzed by ICP-MS (Table S2). The final solid samples were analyzed by EDS and PXRD (Figures S3 and S4).

2.2. Crystallographic Studies and Powder X-ray Diffraction. Diffraction data for CUPB1 were collected on an Agilent Technologies SuperNova diffractometer with Mo−Kα radiation (λ = 0.71073 Å) at room temperature. All data sets were corrected for Lorentz and polarization factors as well as for absorption by the multiscan method.[32a] Structure of compound CUPB1 was solved by direct method and refined by a full-matrix least-squares fitting on F^2 by SHELX-97.[32b] Its structure was checked for possible missing symmetry elements using PLATON with the ADDSYM algorithm, and no higher symmetry was found.[32c] Crystallographic data and structural refinements for CUPB1 are summarized in Table 1. More information on the important bond distances and angles of CUPB1 are listed in Table S1.

https://doi.org/10.1021/acs.inorgchem.5c04481
Inorg. Chem. 2025, 64, 24754−24765

Table 1. Crystal Data and Structure Refinements for Compound CUPB1[a]

compound	CUPB1
FW	3215.02
Space group	$P4_12_12$
a(Å)	12.2376(3)
b(Å)	12.2376(3)
c(Å)	33.9468(11)
α(deg)	90
β(deg)	90
γ(deg)	90
V(Å^3)	5083.8(2)
Z	4
λ(Å)	0.71073
F(000)	5488
D_C(g cm^{-3})	4.201
GOOF on F^2	1.073
R_1	0.0304
wR_2	0.0740

[a] $R_1 = \sum||F_o| - |F_c||/\sum|F_o|$, $wR_2 = \{\sum w[(F_o)^2 - (F_c)^2]^2/\sum w[(F_o)^2]^2\}^{1/2}$

X-ray powder diffraction data were measured on a Bruker-AXS D4 Endeavor diffractometer, 40 kV/40 mA, in Bragg−Brentano geometry. The diffractometer is equipped with a copper X-ray tube and a primary nickel filter producing Cu K$\alpha_{1,2}$ radiation (λ = 1.54187 Å). A linear silicon strip LynxEye detector (Bruker-AXS) was used. Data were recorded in the range of 2θ = 10−80 ° with 10 s/step and a step width of 0.02 °. The aperture of the fixed divergence slit was set to 0.2 mm, and the receiving slit was set to 8.0 mm, respectively. The discriminator of the detector was set to an interval of [0.16−0.25 V].

2.3. Scanning Electron Microscopy (SEM)/Energy-Dispersive X-ray Spectroscopy (EDS) Analyses. Elemental analyses, scanning electron microscopy image, and energy-dispersive X-ray spectroscopy (SEM/EDS) were collected on an FEI Quanta 200F environment scanning electron microscope with a low-vacuum mode at 0.6 mbar. SEM/EDS results are given in the Supporting Information (Figure S3).

2.4. Raman Spectroscopy. Unpolarized Raman spectra were recorded with a Horiba LabRAM HR spectrometer by using a Peltier cooled multichannel CCD detector. An objective lens with a 50× magnification was linked to the spectrometer, allowing the analysis of samples as small as 2 μm in diameter. The samples were in the form of crystals. The incident radiation was produced by a He−Ne laser line at a power of 17 mW (λ = 632.8 nm). The focal length of the spectrometer was 800 mm, and a 1800 gr/mm grating was used. The spectral resolution was approximately 1 cm^{-1} with a slit of 100 μm. The spectrum was recorded in the range of 100−4000 cm^{-1}.

2.5. Thermal Analysis (TG-DSC Experiments). The thermal behavior of the polycrystalline CUPB1 up to 1200 °C was studied by differential scanning calorimetry (DSC) analysis coupled with thermogravimetry (TG) in air at a heating rate of 10 °C/min using a Netzsch STA 449C Jupiter apparatus. The sample (12.5 mg) was loaded into a platinum crucible, which was covered with a platinum cover. During the measurements, a constant air flow of 20−30 mL/min was applied.

2.6. Bond-Valence Analysis. As a semiempirical method for the approximate determination of valence states, BVS of all atoms in phase CUPB1 were calculated and agree well with corresponding formal values of oxidation states. The bond-valence parameters for U(VI)-O, Cs(I)-O, P(V), and B(III)-O were used according to Brese and O'Keeffe.[33] (Table S2)

2.7. Inductively Coupled Plasma Mass Spectrometry (ICP-MS) Analyses. ICP-MS is a type of mass spectrometry that is capable of detecting metals and several nonmetals at concentrations as low as one part in 10^{15} (part per quadrillion, ppq) on noninterfered low-background isotopes.[34] The concentrations of metal ions in the solution before and after ion-exchange experiments were analyzed using PE Sciex ELAN 6100 ICP-MS instrumentation. All samples (including standards) were prepared in a 1% nitric acid solution. All of the ion-exchanged solution samples were diluted to lower the concentrations below 100 ppb for ICP-MS measurements.

3. RESULTS AND DISCUSSION

3.1. Synthesis. The investigation of the Cs−U−P−B-O system, a microporous alkaline metal uranyl borophosphate CUPB1, was carried out in mild hydrothermal conditions. It was prepared by a very simple procedure with starting chemicals in a ratio of $UO_2(NO_3)_2(H_2O)$:H_3BO_3:H_3PO_3:CsOH·x(H_2O) = 1:10:4:4, together with 0.5 mL of deionized water. For understanding the reaction mechanism more clearly, we have performed the following experiments with the different ratios of $UO_2(NO_3)_2(H_2O)_6$:H_3BO_3:H_3PO_3:CsOH·x(H_2O) = 1:1:4:4; 1:3:4:4; 1:5:4:4; 1:8:4:4; 1:10:4:4; 1:12:4:4, and 1:15:4:4. The final results are that we can only get the crystals CUPB1 in the ratios of 1:8:4:4; 1:10:4:4 and 1:12:4:4, in which the highest yield is from the ratio of 1:10:4:4. The main byproducts of the above syntheses are the cesium uranyl phosphate, $Cs_2(UO_2)_2(PO_4)_2$,[31] which is a quite stable phase in this reaction system. Thus, we supposed that H_3BO_3 has

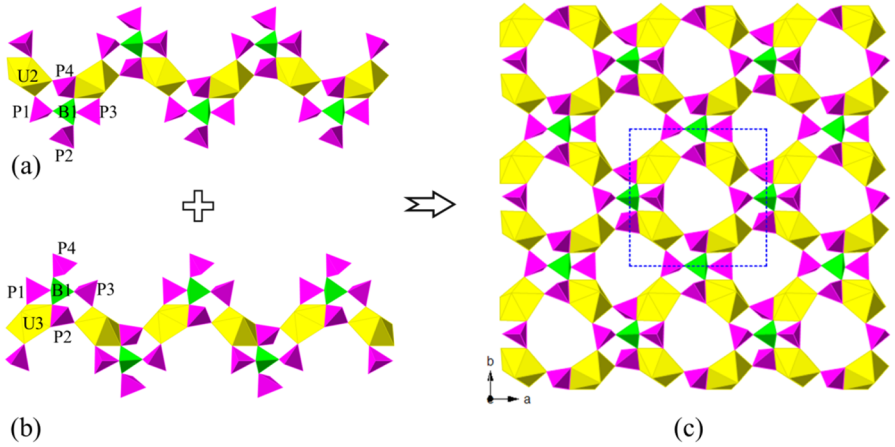

Figure 1. Zigzag uranyl borophosphate chain U(2)B$(PO_4)_4$ (a) and U(3)B$(PO_4)_4$ (b) along the a-axis; a 2D uranyl borophosphate sheet on the ab-plane (c). UO_7 polyhedra, BO_4, and PO_4 tetrahedra are shown in yellow, green, and pink, respectively.

https://doi.org/10.1021/acs.inorgchem.5c04481
Inorg. Chem. 2025, 64, 24754−24765

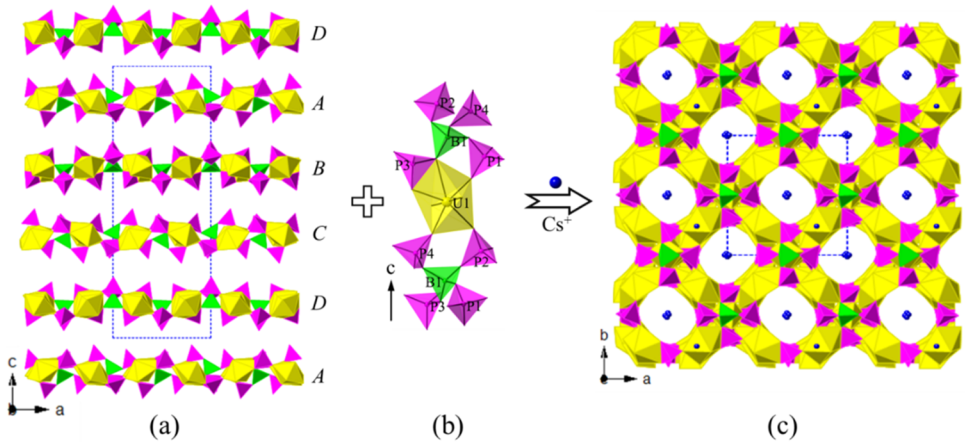

Figure 2. 2D uranyl borophosphate sheets $[U(2/3)B(PO_4)_4]$ are parallel arranged along the *c*-axis (a); 1D $[U(1)B(PO_4)_4]$ chain along the *c*-axis (b); and view of the 3D framework structure of CUPB1 down the *c*-axis (c). UO_7 polyhedra, BO_4, PO_4 tetrahedra, and Cs atoms are shown in yellow, green, pink, and blue, respectively.

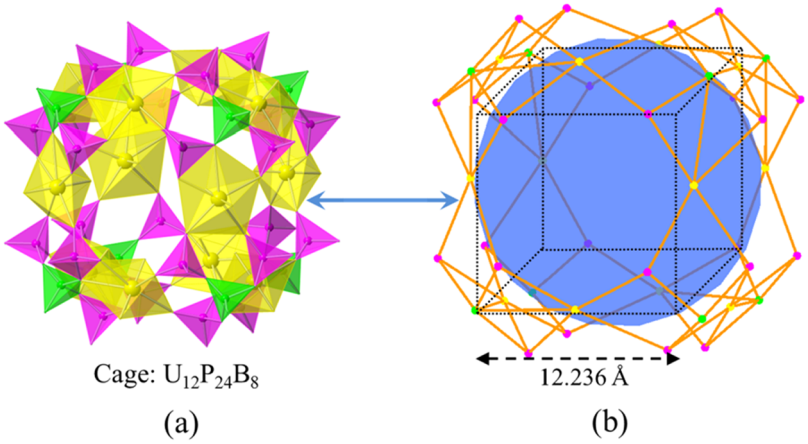

Figure 3. A spherical uranyl borophosphate cage $[U_2P_{24}B_8]$ polyhedral (a) and topology (b) representation. UO_7 polyhedra, BO_4, PO_4 tetrahedra, and Cs atoms are shown in yellow, green, pink, and blue, respectively.

played both important roles of flux and reaction medium in the hydrothermal reactions. Note that the first three actinide borophosphates were prepared with H_3BO_3−$NH_4H_2PO_4$ flux method at around 200 °C with quite less water (50 μL).[29b] Changing from H_3PO_3 to $NH_4H_2PO_4$, the preparation of compound CUPB1 was unsuccessful with powder products, and no crystal phases formed, which indicated that the crystal CUPB1 formation process requires a lower pH value.

3.2.1. Structure of CUPB1. The compound CUPB1 has a unique microporous structure that crystallizes in the chiral space group of $P4_12_12$ (No. 94). There are three Cs, three U, one B, and four P atom positions in the asymmetric unit. CUPB1 is an extremely rare porous borophosphate, which is built from three basic building units (BBU), UO_7 pentagonal bipyramids, BO_4, and PO_4 tetrahedra.[35−37] One BO_4 tetrahedron exhibits corner sharing with four PO_4 tetrahedra, forming the $[B(PO_4)_4]$ clusters. From the fundamental building blocks (FBBs) view, the $[B(PO_4)_4]$ can also be described as (5□:[□]□|□|□|□|) according to the borate classification system.[10] As shown in Figure S4c, the $[B(PO_4)_4]$ FBBs are isolated inside its 3D framework structure, which is similar to the actinide-free borophosphate $Na_3Cd_3B(PO_4)_4$ and $Cs_2Cr_3(BP_4O_{14})(P_4O_{13})$.[38a,b] The $U(2)O_7$ and $U(3)O_7$ pentagonal bipyramids are corner or edge sharing with those $[B(PO_4)_4]$ FBBs forming two mirror symmetric S-type uranyl borophosphate chains, $[U(2)O_2][B(PO_4)_4]$ and $[U(3)O_2][B(PO_4)_4]$ (UBP-chains), along the *a*-axis (Figure 1a,b). The two S-type UBP-chains bridge vertex sharing linked by $[B(PO_4)_4]$ anionic groups, forming a 2D uranyl borophosphate sheet $[U(2)\text{-}BP_4\text{−}U(3)]$ on the *ab*-plane, in which 8-Rings (8-Rs) with four repeated linkages $\text{-}UO_7\text{−}PO_4\text{−}$, can be observed along the *c*-axis (Figure 1c). They paralleled $U(2)\text{-}BP_4\text{−}U(3)$ layers packing in a mode of ---*ABCDA*--- with a periodic time of four. $U(1)O_7$ pentagonal bipyramids acted as the linkers further connected the paralleled $U(2)\text{-}BP_4\text{−}U(3)$ layers along the *c*-axis, constructed its 3D porous uranyl borophosphate framework $[(UO_2)_3B(PO_4)_4]^{3-}$ (Figure 2a,b). Three different multi-intersection 8-R tunnels, running along the [001], [110], and [−110] directions, can be observed in the anionic network. Cs^+ cations are disordered and located in the tunnels and voids of the framework for charge balance (Figure 2c).

The B−O bond lengths in the distorted BO_4 tetrahedron range from 1.38(2) to 1.57(2) Å, and the O−B−O bond angles are in the range of 104.0(10)°−117.1(11)°. For PO_4 tetrahedra, the P−O bond distances are in the range of [1.493(9)−1.604(9) Å], while the O−P−O bond angles range from 99.5(5)° to 113.3(5)°, which are consistent with those of borophosphates reported previously.[2] The axial U−O bond

https://doi.org/10.1021/acs.inorgchem.5c04481
Inorg. Chem. 2025, 64, 24754−24765

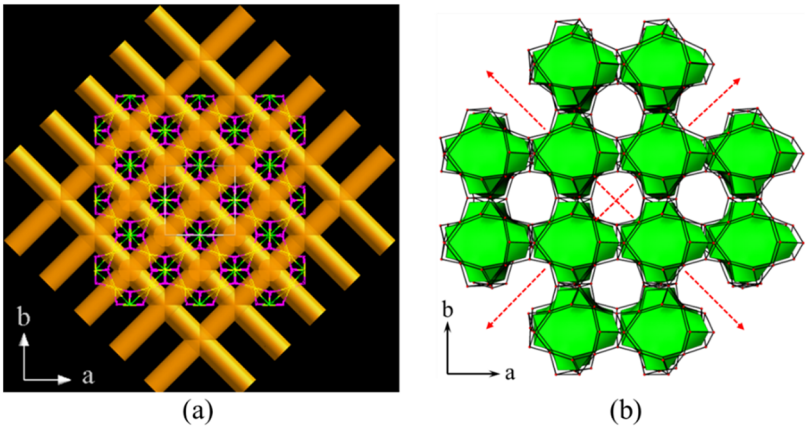

Figure 4. Tracing of the multi-intersection tunnels within the 3D framework of CUPB1 with stick fashion (a) and the $[U_2P_{24}B_8]$-cages packing mode (b).

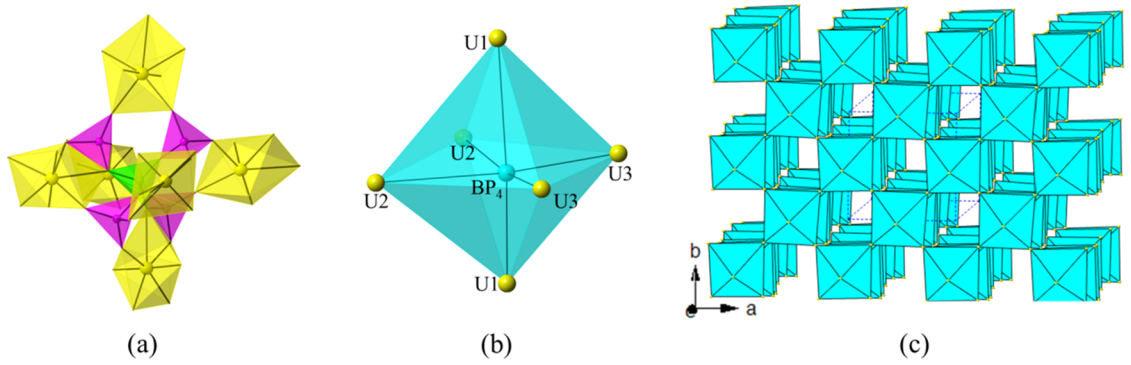

Figure 5. Primary uranyl borophosphate cluster $[(UO_2)_6B(PO_4)_4]$ with B-center (a); a simplified topology of cluster $[(UO_2)_6B(PO_4)_4]$ (square bipyramid geometry) (b); view of the simplified topology representation of CUPB1 down the *c*-axis (c).

lengths for $U(1)O_7$ pentagonal bipyramids are 1.758(10) and 1.768(12) Å, whereas its equatorial U−O bond distances are in the range of [2.284(11)−2.648(9) Å]. The axial U(2)-O bond lengths for $U(2)O_7$ polyhedra are 1.776(9) and 1.775(9) Å, and the equatorial U(2)-O bond distances range from 2.284(8) to 2.648(8) Å. For $U(3)O_7$ pentagonal bipyramids, the axial U(3)-O bond lengths are 1.768(9) Å and 1.781(9) Å, the equatorial U(3)-O bond distances are in the range of [2.274(9)−2.683(8) Å], which are in good agreement with uranyl borates reported earlier[29b,c] (Table S1). The calculated BVS values for B(1), P(1)−P(4), and U(1)−U(3) are ca. 3.04, 5.15, 5.18, 5.21, 5.06, 6.08, 5.99, and 6.0, respectively, which confirmed the valence states of B, P, and U are 3+, 5+, and 6+ in CUPB1. The Cs^+ cations are 10-, 11-, and 12-fold oxygen coordinated, with Cs−O bond lengths from 3.189(9) Å to 3.81(4) Å (Tables S1 and S2)

The key feature of CUPB1 is the nanoscale size cages, $U_{12}P_{24}B_8$, which are built from 12 UO_7 pentagonal bipyramids, 24 PO_4 tetrahedra, as well as eight BO_4 tetrahedra. Its diameters are ∼12.2 Å × 12.2 Å × 11.7 Å and are in a volume of ∼1741.4 $Å^3$. It is the first example of such a large uranyl-based cage containing both PO_4 and BO_4 tetrahedra. The complex $U_{12}P_{24}B_8$ cage has six 8-Rs windows in the six directions of its faces, further bridging connected with six other neighboring ones (Figure 4b). Six Cs^+ cations are located near the windows inside the $U_{12}P_{24}B_8$ cage in a square bipyramid geometry. Compared with those uranyl peroxide cage clusters reported by Burns et al.,[39] the incorporation of BO_4 tetrahedra makes the $U_{12}P_{24}B_8$ cage a more complex topology. Not like the uranyl groups edge sharing with each other to build its hemisphere or even the whole skeleton in U_{28} or $U_{124}P_{32}$ cages,[40] uranyl groups are isolated in the $U_{12}P_{24}B_8$ cages. U(2) and U(3) pentagonal bipyramids linked by $[B(PO_4)_4]$ FBBs, forming the hemisphere, $U_4B_4P_{12}$, of the cage; four U(3) ions in the equatorial line bridge connected with the two symmetric $U_4B_4P_{12}$ hemispheres, creating the unusual nanoscale size uranyl borophosphate cage, $U_{12}P_{24}B_8$ (Figure 3).

3.2.2. Framework Topology Characterization. The 3D anionic framework of CUPB1 is extremely complex and difficult to describe clearly. In order to give a detailed description of the uncommon zeolite-like topology network of CUPB1, the simplified anionic framework $[(UO_2)_3B(PO_4)_4]$ of CUPB1 was plotted through omitting the oxygen anions (Figure S5). The simplified cationic net of CUPB1 can be described as a new 8-nodal net topological type with a Schläfli symbol of $\{3.4^2.5^2.6\}_3\{3^2.4^2.8^3.9^3\}_3\{3^3.4^3\}\{3^6.4^9.5^6\}$[41] (Figure 4a,b). The 3D porous framework of CUPB1 has a low framework density of ∼12.6 M atoms (M is the cations of the framework) per 1000 $Å^3$, which is even lower than the open zeolite faujasite with framework density of ∼13.5.[42a] Each of the UO_7 pentagonal bipyramid is surrounded by two $[B(PO_4)_4]$ FBBs, whereas six UO_7 pentagonal bipyramids are sitting around each $[B(PO_4)_4]$ FBB unit (note as *X* here), existing as a XU_6 square bipyramid geometry. Thus, the ratio of *X* and U is 1:3 in a XU_3 network structure (Figure 5). If we simplified the porous anionic framework $[(UO_2)_3B(PO_4)_4]^{3-}$ of CUPB1 with FBB $[B(PO_4)_4]$ as a 6-connected node (*X*) in the 3D network, we can get a XU_3 topology network as shown

https://doi.org/10.1021/acs.inorgchem.5c04481
Inorg. Chem. 2025, 64, 24754−24765

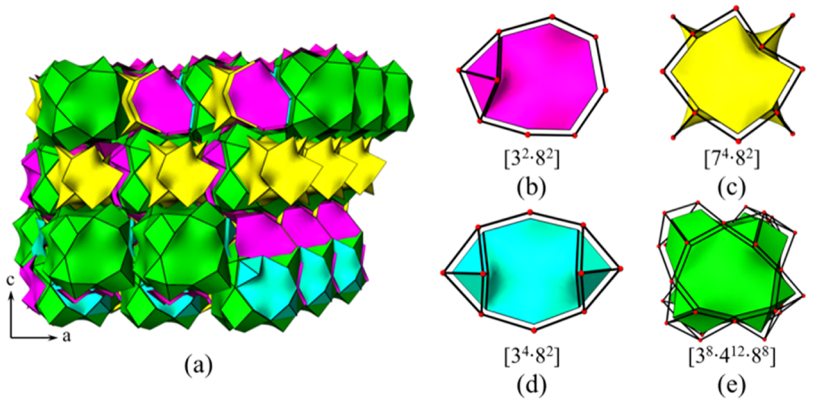

Figure 6. View of the 3D framework structure of CUPB1 using tiling (a) and the basic tiles of its tiling structure $[3^2{\cdot}8^2]$ (b), $[7^4{\cdot}8^2]$ (c), $[3^4{\cdot}8^2]$ (d), and $[3^8{\cdot}4^{12}{\cdot}8^8]$ (e).

in Figure S6a,b,c; this simplified cationic net is a new 2-nodal net topological type with the Schläfli symbol of $\{8^{12}.12^3\}\{8\}_3$[41] (Figure S6).

The channel system and cavities of CUPB1 can be better illustrated by natural tiling by tracing the colors of the tiles. From the natural tiling point of view, the anionic uranyl borophosphate framework of CUPB1 is built from four different tiles, in which the primary build unit (PBU) is the cage $[7^4{\cdot}8^2]$. These $[7^4{\cdot}8^2]$ PBUs connected with four other neighboring ones on the *ab*-plane; leave a large hole surrounded by four $[7^4{\cdot}8^2]$ cages. These large cavities were filled with another nanosize cage $[3^8{\cdot}4^{12}{\cdot}8^8]$ bridged by the tile of $[3^4{\cdot}8^2]$, defining a 2D layer parallel with the ab-plane. Those paralleled 2D layers were further linked by a $[3^2{\cdot}8^2]$ tile, forming its extraordinary 3D tiling frameworks. From the tiling model of CUPB1, it is easier to trace its tunnels, cages, and cavities with tiling signatures of $[7^4{\cdot}8^2]$ + $[3^8{\cdot}4^{12}{\cdot}8^8]$ + $[3^4{\cdot}8^2]$ + $[3^2{\cdot}8^2]$ (Figures 6 and S6).

3.3.1. Ion-Exchange Properties. CUPB1 is an exceedingly porous material with a high free void volume within its 3D open framework structures. Furthermore, the Cs^+ ions are disordered and reside in the free voids of the porous network; these have prompted us to investigate their ion-exchange properties.[43,44] Ion-exchange experiments were conducted with a variety of cations, from monovalent A^+ to tetravalent A^{4+} at room temperature and elevated temperatures. CUPB1 has shown significant ion-exchange properties with A^{2+}. The ion-exchanged samples were further studied by EDS elemental analyses, element distribution mapping, ICP-MS analyses, as well as powder X-ray diffraction (PXRD).[45] From the PXRD patterns, we can see that the framework structure of CUPB1 remains intact after the ion-exchange experiments, which has the same characteristics as the reported zeolites and MOF materials[3] (Figures S2 and S3, Table S2). Compared with porous zeolites and MOFs reported in the literature, we note that while zeolites[4] and MOFs[5,6] often have higher capacities due to their microporosity, CUPB1 offers distinct advantages: (1) exceptional selectivity for large, hard cations like Sr^{2+}, Ni^{2+}, etc., and (2) high chemical and potential radiation stability inherent to inorganic uranium phases. This positions CUPB1 as a specialized ion exchanger for challenging environments, where stability is paramount.

3.3.2. Kinetic Studies of the Cations A^{2+} (A = Sr, Ba, Pb, Co, Ni) Exchange. Sorbents are particularly desirable, since they can adsorb the very toxic ions, such as Pb^{2+}, Ni^{2+}, Co^{2+}, etc.,[42b,c] and some radionuclides, such as ^{137}Cs, ^{90}Sr, ^{137m}Ba, etc.[42d,e] Because CUPB1 has promising ion-exchange results as described above, we explored in more detail the toxic cation remediation properties. The kinetics of Sr^{2+} ion-exchange was investigated, and it was shown that the concentrations of Sr^{2+} (~450 ppm at a V/m ratio of 200 mL/g) decreased rapidly: the relative amount of Sr-removed reached ~56% after 24 h and increased to ~70.2% after 74 h at room temperature (Figure 9a and Table S2). Based on eq 1, we can calculate the Sr-exchange capacity q^{Sr} is ~64.1 mg/g. The distribution coefficient K_d is a measurement of affinity and selectivity shown as eq 2. The Sr-exchanged K_d^{Sr} at RT for CUPB1 is 493.3 mL/g. It is interesting to note that, when the temperature increases to 70 °C, both the q^{Sr} and K_d^{Sr} have improved to 74.2 mg/g and 942.8 mL/g, respectively (Figure 9a and Table S2). The Sr-removed amount R increased up to 82.9% after 72 h, which is comparable with the Sr-exchangers reported previously.[46]

We argue that temperature is one of the important driving forces for ion-exchange reactions. Similarly, we have performed Ba-exchange experiments with Sr^{2+} in the same conditions.[47,48] The calculated Ba-exchange capacity of q^{Ba} is ~100.4 mg/g and K_d^{Ba} of ~498.6 mL/g based on eqs 1, 2, and 3 at RT.[49] As expected, both the q^{Ba} and K_d^{Ba} improved to ~113.4 mg/g and ~830.3 mL/g at 70 °C, and the Ba-removed amount approached ~80.7% (Figure 9b and Table S2). For comparison, the relative Sr-exchange properties of CUPB1 are better than the Ba ones. We assumed that because the radius of Sr^{2+} is smaller than that of Ba^{2+} cations, the Sr-exchange mechanism needs a lower adsorption energy.[33] The ionic radii for cations are Cs^+ (~1.69 Å), Sr^{2+} (~1.26 Å), and Ba^{2+}(~1.42 Å). While Ba^{2+} is smaller than Cs^+, its size is still relatively larger than that of Sr^{2+} for the channels in CUPB1. More importantly, the driving force for exchange is a combination of hydration energy and lattice energy. Sr^{2+} has a charge density much higher than that of Ba^{2+}, leading to a more negative hydration energy. This makes the dehydration of Sr^{2+} (a necessary step for entering the crystal lattice) less favorable, but once inside, its higher charge provides a stronger electrostatic interaction with the anionic framework, which likely dominates the thermodynamics for this system. The larger Ba^{2+} may experience greater steric hindrance within the channels, slowing its diffusion and reducing the overall exchange capacity. We presume that the optimal fit and stronger Coulombic attraction for Sr^{2+} likely explain its higher exchange rate.

https://doi.org/10.1021/acs.inorgchem.5c04481
Inorg. Chem. 2025, 64, 24754−24765

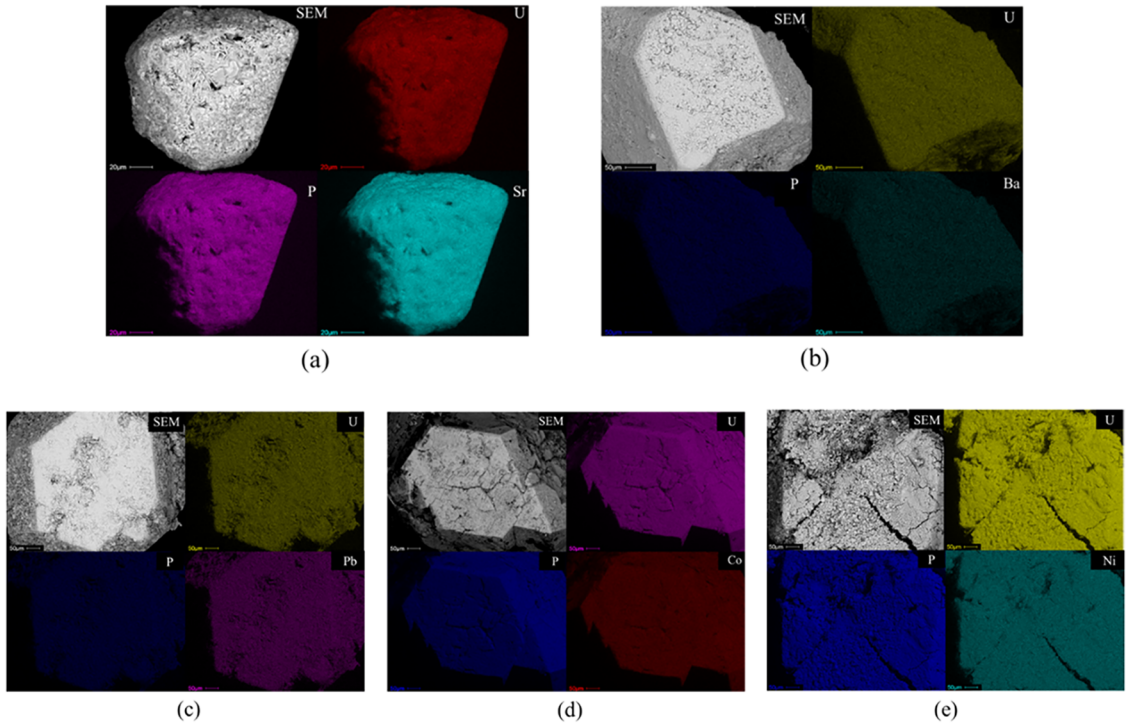

Figure 7. SEM image of the Sr (a), Ba (b), Pb (c), Co (d), and Ni (e)-exchanged samples and elemental distribution maps.

Figure 8. Photos of CUPB1 crystals before and after colored ions (Co^{2+} and Ni^{2+}) exchanged samples.

$$q = \frac{(C_0 - C_e)V}{m} \quad (1)$$

$$K_d = \frac{V}{m}\frac{(C_0 - C_f)}{C_f} \quad (2)$$

$$R = \frac{(C_0 - C_f)}{C_0} \quad (3)$$

In eqs 1, 2, and 3, C_0 and C_f represent the initial and equilibrium concentrations of the ions as measured by ICP-MS, V is the solution volume, m is the mass of CUPB1, and R is the relative amount of cation removed.

Heavy metal ions in solution are toxic to humans if the concentration is sufficiently high. For example, Pb is a highly poisonous metal (whether inhaled or swallowed), affecting almost every organ and system in the human body.[50a] Therefore, during the last decades, how to separate the toxic ions from the solutions efficiently is a one of the core questions.[50] Removal of inorganic pollutants from the aqua can be achieved by electrodialysis,[50b] chemical precipitation,[50c] adsorption,[50d] solvent extraction,[50e] and ultrafiltration[50f] or ion exchange.[50g] CUPB1 shows a promising application for ion exchange with Pb^{2+} from Pb-contaminated solutions. The kinetics of Pb^{2+} ion-exchange showed that the Pb amount (~950 ppm at a V/m ratio of 200 mL/g) decreased ~76.9% after 72 h at RT. The Pb-removed amount has increased to 83.6% at the temperature of 70 °C (Figure 9c and Table S2). The Pb-exchange capacity of q^{Pb} is ~146.4 mg/g at RT and ~169.4 mg/g at 70 °C. The K_d^{Pb} at RT is 720 mL/g, whereas the higher K_d^{Pb} value reached 1640 mL/g at 70 °C (Figure 9c and Table S2). The promising Pb-exchanged properties of CUPB1 are comparable with those previously reported modified zeolites[34b,c] and resins (Figure 7).[33]

There are groups of divalent transition-metal cations (Co^{2+}, Ni^{2+}, Zn^{2+}, Cu^{2+}, *etc.*) exchangers that have been synthesized and characterized, such as resins,[51a] MOFs,[51b] zeolites or zeolite-like materials,[51c] and polymers.[51d] Among them, MOFs, zeolites, or zeolite-like materials preserve their original crystal structure after ion-exchange reactions, which resembles CUPB1.[52−54] As shown in Figure 8, the CUPB1 crystals show the colors of the transition metals (Co^{2+} and Ni^{2+}) within a few days. The crystals can be cut, and the interior shows the same color as the surface. EDS, elemental distribution maps, and ICP-MS data were collected from crystals and the solutions after exchange, and these can demonstrate the presence of the cations within the crystals (Figure S3 in the Supporting Information).[55,56] CUPB1 exhibits a better Co^{2+} adsorption at a higher temperature of 70 °C (R~74% after 72 h) compared to the RT (R~64%). Accordingly, the exchange capacity q^{Co} is ~44.4 mg/g at 70 °C, higher than that at ~38.6

https://doi.org/10.1021/acs.inorgchem.5c04481
Inorg. Chem. 2025, 64, 24754−24765

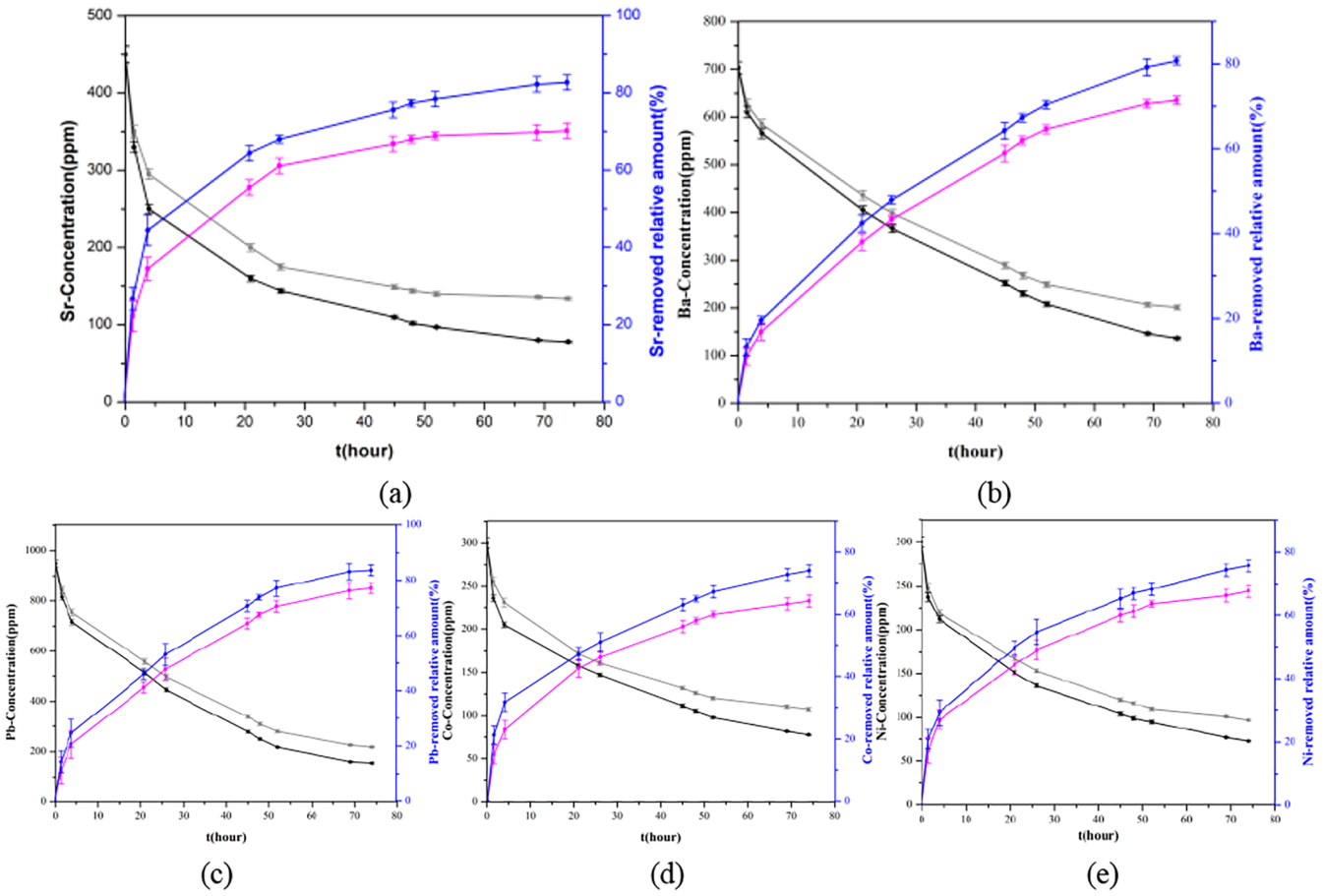

Figure 9. Kinetics of the A^{2+} ($Sr^{2+}/Ba^{2+}/Pb^{2+}/Co^{2+}/Ni^{2+}$) ion-exchanged with 50 mg of CUPB1 (A: Cs = 1:2) plotted as the A-concentration (ppm) (black/gray line) and the relative A-removed amount (%) (blue/pink line) vs time t (hour), respectively, (a–e). Pink and gray represent reaction at RT, and black and blue are at 70 °C.

mg/g at RT. The distribution coefficient K_d^{Co} increased to 569.2 mL/g (70 °C) from 355.6 mL/g (RT) (Figure 9d and Table S2). The maximum Ni^{2+} exchange capacity q^{Ni} of CUPB1 was found to be ~40.6 mg/g at RT, the corresponding removed amount is ~67.7% and the K_d^{Ni} is ~ 425.1 mL/g. When the exchanged temperature increased up to 70 °C, the q^{Ni} and K_d^{Ni} can be as high as ~45.4 mg/g and ~633.3 mL/g, respectively (Figure 9e and Table S2).

3.4. Thermal Analysis. Thermogravimetric (TG) and differential scanning calorimetry (DSC) measurements were performed from 50 to 1200 °C (Figure S9). TG analysis indicates that CUPB1 shows no obvious weight loss until 1000 °C.[57−59] There is a small endothermic peak at 387 °C that can be assigned to the removal of 0.5 mol of water molecules per formula unit, which is too light to be shown in the TG curve. The endothermic peak at 835 °C is matched with the decomposition of the anhydrate phases. From the thermal behavior of CUPB1, we concluded that its porous framework is robust and stable.

3.5. Raman Analysis. The Raman spectra of CUPB1 and its ionic exchange products were measured in a range of 100−4000 cm^{-1}, and for convenience, we have divided the spectra into two sections: a low-frequency part in 100−1300 cm^{-1} and a high-frequency region in 3000−4000 cm^{-1} (Figure S10). After comparison, the Raman spectra of CUPB1 and the ion-exchanged samples show no obvious difference, which confirms that the 3D uranyl borate framework is intact after ion-exchange experiments. More scattering peaks are in the range of 100−1000 cm^{-1}, which is dominated by contributions from the $(UO_2)^{2+}$, BO_3 triangles and BO_4, PO_4 tetrahedra modes of CUPB1. The Raman bands located in lower frequencies in the range of 190−300 cm^{-1} could be attributed to the uranyl ion with a υ_2 bending mode.[60,61] Raman bands with a series of peaks around 476 cm^{-1} could be assigned to O−B−O doubly degenerated symmetric bending ν_2 mode in BO_4 tetrahedra. The Raman peak at ~642 cm^{-1} is attributed to the bending character ν_4 of BO_4. Raman bands from 800 to 870 cm^{-1} come from the symmetric vibration υ_1 mode of the uranyl $(UO_2)^{2+}$ units. The characteristic vibrations of uranyl $(UO_2)^{2+}$ υ_3 antisymmetrical stretch mode are at bands of 936 cm^{-1} and 978 cm^{-1}. The Raman bands at 1002 cm^{-1} and 1018 cm^{-1} can be attributed to the ν_1 PO_4 symmetric stretching and ν_3 PO_4 antisymmetric stretching modes. The Raman bands within 1100−1200 cm^{-1} can be attributed to the O−B−O triply degenerated asymmetric mode stretching ν_3 mode in BO_4 tetrahedra. These assignments are consistent with previously reported works.[62]

4. CONCLUSIONS

A remarkable ion exchanger CUPB1 was obtained from the mild hydrothermal method. Its microporous framework is based on the FBBs of the $[B(PO_4)_4]^{9-}$ and UO_7 pentagonal bipyramids. The unusual nanoscale size (~12.2 × 12.2 × 11.7 Å) of uranyl borophosphate cages, $U_{12}P_{24}B_8$, is observed in the

https://doi.org/10.1021/acs.inorgchem.5c04481
Inorg. Chem. 2025, 64, 24754−24765

network structure. In its 3D open framework, there are three multi-intersection 8-R tunnels along the [001], [110], and [-110] directions. The disordered Cs^+ cations reside in the tunnels and voids of the framework. Its free void volume is as high as ∼59%, which demonstrates it is an extremely high porous actinide compound. From the topological viewpoint, the 3D porous framework of CUPB1 has a very low framework density of ∼12.6 M atoms per 1000 $Å^3$, which is comparable with the typical zeolite materials. Importantly, as a highly porous material, CUPB1 can adsorb the cations from monovalent to divalent in solution at room or elevated temperatures. The remarkable ion-exchange properties of CUPB1 can be attributed to its open framework with three-dimensional chiral channels and disordered guest cations. We have studied the ion-exchange properties of CUPB1 with some toxic metal cations, Pb^{2+}, Co^{2+}, and Ni^{2+} and important nuclear fission products of Sr^{2+} and Ba^{2+}, at both room temperature and 70 °C. This has proved that CUPB1 is a promising potential ion exchanger for the separation or purification of the toxic cations and nuclear wastes contaminated waters. The ion-exchange properties of CUPB1 have improved a certain point for all the cation-exchanged experiments at a higher temperature of 70 °C. At RT, the ion-exchange capacity q for Sr^{2+}, Ba^{2+}, Pb^{2+}, Co^{2+}, and Ni^{2+} is ∼64.1, ∼100.4, ∼146.4, ∼38.6, and ∼40.6 mg/g, respectively. When the temperature increased to 70 °C, the q improved to ∼74.2, ∼113.4, ∼169.4, ∼44.4, and ∼45.4 mg/g. This study has demonstrated the excellent thermal stability of the CUPB1 framework structure. Further investigations of the monovalent cations, such as Li^+, Na^+, K^+, Rb^+, NH_4^+, etc., and uranyl borophosphate analogues of CUPB1 are underway.

■ ASSOCIATED CONTENT

Supporting Information

The Supporting Information is available free of charge at https://pubs.acs.org/doi/10.1021/acs.inorgchem.5c04481.

Selected bond lengths and angles, topological figures, PXRD patterns, SEM-EDS measurements, ICP-MS data, TG-DSC curves, and Raman spectra (PDF)

Accession Codes

Deposition Number 2487026 contains the supplementary crystallographic data for this paper. These data can be obtained free of charge via the joint Cambridge Crystallographic Data Centre (CCDC) and Fachinformationszentrum Karlsruhe Access Structures service.

■ AUTHOR INFORMATION

Corresponding Authors

Yucheng Hao − *School of Energy Materials and Chemical Engineering, Hefei University, Hefei 230000, China;* orcid.org/0000-0001-5281-1751; Email: haoyco@hfuu.edu.cn

Evgeny V. Alekseev − *Institute of Energy Technologies (IET-1), Forschungszentrum Jülich GmbH, 52428 Jülich, Germany;* orcid.org/0000-0002-4919-5211; Email: e.alekseev@fz-juelich.de

Authors

Xu Jingli − *School of Energy Materials and Chemical Engineering, Hefei University, Hefei 230000, China*

Thomas E. Albrecht − *Department of Chemistry and Nuclear Science and Engineering Center, Colorado School of Mines, Golden, Colorado 80401, United States;* orcid.org/0000-0002-2989-3311

Shuao Wang − *School for Radiological and Interdisciplinary Sciences (RAD-X) and Collaborative Innovation Center of Radiation Medicine of Jiangsu Higher Education Institutions, Suzhou, Jiangsu 215123, China;* orcid.org/0000-0002-1526-1102

Rüdiger-A. Eichel − *Institute of Energy Technologies (IET-1), Forschungszentrum Jülich GmbH, 52428 Jülich, Germany;* orcid.org/0000-0002-0013-6325

Complete contact information is available at: https://pubs.acs.org/10.1021/acs.inorgchem.5c04481

Notes

The authors declare no competing financial interest.

■ ACKNOWLEDGMENTS

The authors are grateful to Anhui New Era Education Quality Project for Graduate (2022qyw/sysfkc042); Anhui Provincial Traditional Professional Transformation and Upgrading Project (2023zygzts043); Hefei University Teaching Research Project (2023hfujyyb15); Anhui Provincial Quality Engineering Project (2024fwxx032); and Funding of Nanjing Weizhi Biotechnology Co., Ltd. (902/22050125011). We are thankful to Dr. Philip Kegler and Dr. Martina Klinkenberg for their help in data collection.

■ REFERENCES

(1) (a) Cheetham, A. K.; Férey, G.; Loiseau, T. Open-Framework Inorganic Materials. *Angew. Chem., Int. Ed.* **1999**, *38*, 3268−3292. (b) James, S. L. Metal-organic frameworks. *Chem. Soc. Rev.* **2003**, *32*, 276−288. (c) Maspoch, D.; Ruiz-Molina, D.; Veciana, J. Old materials with new tricks: multifunctional open-framework materials. *Chem. Soc. Rev.* **2007**, *36*, 770−818. (d) Slater, A. G.; Cooper, A. I. Function-led design of new porous materials. *Science* **2015**, *348*, No. aaa8075.

(2) (a) Plabst, M.; McCusker, L. B.; Bein, T. Exceptional ion-exchange selectivity in a flexible open framework lanthanum(III)-tetrakisphosphonate. *J. Am. Chem. Soc.* **2009**, *131*, 18112−18118. (b) Choi, H. J.; Suh, M. P. A Robust Porous Material Constructed of Linear Coordination Polymer Chains: Reversible Single-Crystal to Single-Crystal Transformations upon Dehydration and Rehydration. *J. Am. Chem. Soc.* **2004**, *126*, 15844−15851. (c) Rowsell, J. L. C.; Yaghi, O. M. Strategies for Hydrogen Storage in Metal—Organic Frameworks. *Angew. Chem., Int. Ed.* **2005**, *44*, 4670−4679. (d) Cheetham, A. K.; Rao, C. N. R.; Feller, R. K. Structural Diversity and Chemical Trends in Hybrid Inorganic—Organic Framework Materials. *Chem. Commun.* **2006**, *46*, 4780−4795. (e) Seo, J. S.; Whang, D.; Lee, H.; Im Jun, S.; Oh, J.; Jeon, Y. J.; Kim, K. A homochiral metal-organic porous material for enantioselective separation and catalysis. *Nature* **2000**, *404*, 982−986. (f) Maspoch, D.; Ruiz-Molina, D.; Veciana, J. Old materials with new tricks: multifunctional open-framework materials. *Chem. Soc. Rev.* **2007**, *36*, 770−818.

(3) (a) http://www.iza-structure.org/databases/;. (b) Rowsell, J. L.; Yaghi, O. M. Exploratory study of mesopore templating with carbon during zeolite synthesis. *Microporous Mesoporous Mater.* **2004**, *73*, 3−14.

(4) (a) Zhang, Z.; Han, Y.; F Xiao, S.; Qiu, S.; Zhu, L.; Wang, R.; Yu, Y.; Zhang, Z.; Zou, B.; Wang, Y.; Sun, H. Mesoporous Aluminosilicates with Ordered Hexagonal Structure, Strong Acidity, and Extraordinary Hydrothermal Stability at High Temperatures. *J. Am. Chem. Soc.* **2001**, *123*, 5014−5021. (b) Wang, J.; Zhang, Y.; Zhang, Z.; Xu, Y. Synthesis and structural characterization of three 3-D aluminogermanates with different topologies. *CrystEngComm* **2014**, *16*, 5103−5109. (c) Yu, J.; Xu, R. Insight into the construction of open-framework aluminophosphates. *Chem. Soc. Rev.* **2006**, *35*, 593−604.

(5) (a) Burrows, A. D.; Hunter, S. O.; Mahon, M. F.; Richardson, C. A reagentless thermal post-synthetic rearrangement of an allyloxy-tagged metal−organic framework. *Chem. Commun.* **2013**, *49*, 990−992. (b) Bosch, M.; Zhang, M.; Zhou, H. C. Increasing the Stability of Metal-Organic Frameworks. *Adv. Chem.* **2014**, *2014* (1), No. 182327.
(6) Altınçekiç, N. G.; Lander, C. W.; Roslend, A.; Yu, J.; Shao, Y.; Noh, H. Electrochemically Determined and Structurally Justified Thermochemistry of H atom Transfer on Ti-Oxo Nodes of the Colloidal Metal−Organic Framework Ti-MIL-125. *J. Am. Chem. Soc.* **2024**, *146* (49), 33485−33498.
(7) (a) Szostak, R. *Mokculur Sieves. Principles of Synthesis and Identification*; Van Nostrand Reinhold: New York, 1989. (b) Harrison, W. T.; Gier, T. E.; Stucky, G. D. Tetrahedral-Atom 3-Ring Groupings in One-Dimensional Inorganic Chains: Be_2AsO_4OH-$4H_2O$ and Na_2ZnPO_4OH-$7H_2O$. *Angew. Chem., Int. Ed.* **1993**, *32*, 724−726.
(8) Hao, Y.-C.; He, L.-B.; Ge, G.-J.; Zhang, Q.-Z.; Luo, N.-J.; Huang, S.-P.; Li, H.-J.; Alekseev, Evgeny V. $Mg_3Pt(BO_3)_2O_2$: The first platinum borate from the flux technique. *J. Am. Chem. Soc.* **2020**, *281*, No. 121046.
(9) (a) Krivovichev, S. V.; Kahlenberg, V.; Kaindl, R.; et al. Nanoscale Tubules in Uranyl Selenates. *Angew. Chem., Int. Ed.* **2005**, *44*, 1134−1136. (b) Hao, Y. C.; Xu, X.; Kong, F.; Song, J. L.; Mao, J. G. $PbCd_2B_6O_{12}$ and $EuZnB_5O_{10}$: syntheses, crystal structures and characterizations of two new mixed metal borates. *CrystEngComm* **2014**, *16*, 7689−7695.
(10) (a) Burns, P. C.; Grice, J.; Hawthorne, F. Borate Minerals. I. Polyhedml Clusters And Fundamental Building Blocks. *Can. Mineral.* **1995**, *33*, 1131−1151. (b) Burns, P. C. Borate clusters and fundamental building blocks containing four polyhedra: why few clusters are utilized as fundamental building blocks of structures. *Can. Mineral.* **1995**, *33*, 1167−1176. (c) Jin, S.; Cai, G.; Wang, W.; He, M.; Wang, S.; Chen, X. Li3CaB2O5 F: a unique sandwich-like structure with diverse and wide Li ion diffusion pathways. *Angew. Chem., Int. Ed.* **2010**, *49*, 4967−4970.
(11) Smith-Verdier, P.; Garcia-Blanco, S. Synthesis of the mono (dewar benzene) isomer of [1.1] metacyclophane. *Z. Kristallogr. - Cryst. Mater.* **1980**, *151*, 175−177.
(12) Hao, Y.; Chen, C.; Hou, C.; Liu, S.; Peng, Z.; Lin, Y.; Li, H.; Zhao, X.; Koirala, K.; Lu, H.; Deng, C.; Hu, K. $Li_3[AlP_2O_7F(OH)]$-$(H_2O)_{0.5}$ and $A[Al_2(PO_4)_2F(H_2O)]$(A = K, Rb): Counter Cation Templates Derived Three Polar Alkaline Metal Fluoroaluminophosphates. *Inorg. Chem.* **2024**, *63*, 24885−24895.
(13) Luger, S.; Felsche, J.; Fischer, P. Burnout in Gastroenterology Unit Nurses. *Acta Crystallogr., Sect. C:Cryst. Struct. Commun.* **1987**, *43*, 1−3.
(14) Rowsell, J. L. C.; Taylor, N. J.; Nazar, L. F. Structure and Ion Exchange Properties of a New Cobalt Borate with a Tunnel Structure "Templated" by Na^+. *J. Am. Chem. Soc.* **2002**, *124*, 6522−6523.
(15) (a) Wang, S.; Alekseev, E. V.; Diwu, J.; Casey, W. H.; Phillips, B. L.; Depmeier, W.; Albrecht-Schmitt, T. E. NDTB-1: a super-tetrahedral cationic framework that removes TcO4- from solution. *Angew. Chem., Int. Ed.* **2010**, *49*, 1057−1078. (b) Wang, S.; Yu, P.; Purse, B. A.; Orta, M. J.; Diwu, J.; Casey, W. H.; Phillips, B. L.; Alekseev, E. V.; Depmeier, W.; Hobbs, D. T.; AlbrechtSchmitt, T. E. The Synergistic Effect of Valsartan and LAF237 [(S)-1-[(3-Hydroxy-l-Adamantyl)Ammo]acetyl-2-Cyanopyrrolidine] on Vascular Oxidative Stress and Inflammation in Type 2 Diabetic Mice. *Adv. Funct. Mater.* **2012**, *22*, 2241−2250.
(16) Hao, Y.-C.; Chen, Y.-j.; Cao, X.; Chen, C.; Xu, M.; Lin, Y.; Li, H.; Hu, K. First Potassium Fluoroaluminate Ionic Exchanger for Rapid and Selective Removal of Sr^{2+} with High Capacity. *Chem. - Eur. J.* **2024**, *30*, No. e202400261, DOI: 10.1002/chem.202400261.
(17) (a) Hunt, J. R.; Doonan, C. J.; LeVangie, J. D.; Côté, A. P.; Yaghi, O. M. Reticular synthesis of covalent organic borosilicate frameworks. *J. Am. Chem. Soc.* **2008**, *130*, 11872−11873. (b) Ju, J.; Lin, J.; Li, G.; Yang, T.; Li, H.; Liao, F.; Loong, C. K.; You, L. Aluminoborate-Based Molecular Sieves with 18-Octahedral-Atom Tunnels. *Angew. Chem., Int. Ed.* **2003**, *42*, 5607−5610. (c) Zhang, J.-H.; Kong, F.; Xu, X.; Mao, J. G. Crystal structures and second-order NLO properties of borogermanates. *J. Solid State Chem.* **2012**, *195*, 63−72. (d) Sevov, S. C. Synthesis and Structure of $CoB_2P_3O_{12}(OH)\cdot C_2H_{10}N_2$: The First Metal Borophosphate with an Open Framework Structure. *Angew. Chem., Int. Ed.* **1996**, *35*, 2630−2632. (e) Wiggin, S. B.; Weller, M. T. Boroarsenates: A framework motif and family templated on cations and anions. *J. Am. Chem. Soc.* **2005**, *127*, 17172−17173.
(18) Hao, Y.-C.; Xu, X.; Kong, F.; Song, J.-L.; Mao, J.-G. $PbCd_2B_6O_{12}$ and $EuZnB_5O_{10}$: syntheses, crystal structures and characterizations of two new mixed metal borates. *CrystEngComm* **2014**, *16* (33), 7689−7695.
(19) Wu, H.; Yu, H.; Pan, S.; Huang, Z.; Yang, Z.; Su, X.; Poeppelmeier, K. R. $Cs_2B_4SiO_9$: A Deep-Ultraviolet Nonlinear Optical Crystal. *Angew. Chem., Int. Ed.* **2013**, *125* (12), 3490−3494.
(20) Cao, G.-J.; Wei, Q.; Cheng, J.-W.; Cheng, L.; Yang, G.-Y. A zeolite CAN-type aluminoborate with gigantic 24-ring channels. *Chem. Commun.* **2016**, *52*, 1729−1732.
(21) Hao, Y.-C.; Hu, C.-L.; Xu, X.; Kong, F.; Mao, J.-G. $SrGe_2B_2O_8$ and $Sr_3Ge_2B_6O_{16}$: Novel Strontium Borogermanates with Three-Dimensional and Layered Anionic Architectures. *Inorg. Chem.* **2013**, *52*, 13644−1650.
(22) Zang, Y.; Yu, Y.; Chen, Y.; Fan, M.; Wang, J.; Liu, J.; Xu, L.; Jia, H.; Dong, S. Synthesis of conjugated microporous polymers rich in sulfonic acid groups for the highly efficient adsorption of Cs^+. *Chem. Eng. J.* **2024**, *484*, No. 149709.
(23) (a) Ewald, B.; Huang, Y. X.; Kniep, R. Structural chemistry of borophosphates, metalloborophosphates, and related compounds. *Z. Anorg. Allg. Chem.* **2007**, *633*, 1517−1540. (b) Li, M.; Verena-Mudring, A. New developments in the synthesis, structure, and applications of borophosphates and metalloborophosphates. *Cryst. Growth Des.* **2016**, *16*, 2441−2458.
(24) Sevov, S. C. Synthesis and Structure of $CoB_2P_3O_{12}(OH)\cdot C_2H_{10}N_2$: The First Metal Borophosphate with an Open Framework Structure. *Angew. Chem., Int. Ed.* **1996**, *35*, 2630−2632.
(25) (a) Zhang, H.; Chen, Z.; Weng, L.; Zhou, Y.; Zhao, D. Hydrothermal synthesis of new berylloborophosphates MIBeBPO (MI= K^+, Na^+ and NH^{4+}) with zeolite ANA framework topology. *Microporous Mesoporous Mater.* **2003**, *57*, 309−316. (b) Zhao, D.; Cheng, W. D.; Zhang, H.; Huang, S. P.; Xie, Z.; Zhang, W. L.; Yang, S. L. $KMBP_2O_8$ (M = Sr, Ba): A New Kind of Noncentrosymmetry Borophosphate with the Three-Dimensional Diamond-like Framework. *Inorg. Chem.* **2009**, *48*, 6623−6629. (c) Su, T.; Xing, H.; Xu, J.; Yu, J.; Xu, R. Ionothermal syntheses and characterizations of new open-framework metal borophosphat. *Inorg. Chem.* **2011**, *50*, 1073−1078. (d) Zhang, W.; Cheng, W.; Zhang, H.; Geng, L.; Li, Y.; Lin, C.; He, Z. Syntheses and Characterizations of $Cs_2Cr_3(BP_4O_{14})(P_4O_{13})$ and $CsFe(BP_3O_{11})$ Compounds with Novel Borophosphate Anionic Partial Structures. *Inorg. Chem.* **2010**, *49*, 2550−2556. (e) Zhou, Y.; Hoffmann, S.; Huang, Y. X.; Prots, Y.; Schnelle, W.; Menezes, P. W.; Carrillo-Cabrera, W.; Sichelschmidt, J.; Mi, J. X.; Kniep, R. $K_3Ln[OB(OH)_2]_2[HOPO_3]_2$ (Ln= Yb, Lu): Layered rare-earth dihydrogen borate monohydrogen phosphates. *J. Solid State Chem.* **2011**, *184*, 1517−1522. (f) Yang, W.; Li, J.; Na, T.; Xu, J.; Wang, L.; Yu, J.; Xu, R. $(NH_4)_6[Mn_3B_6P_9O_{36}(OH)_3]\cdot 4H_2O$: A new open-framework manganese borophosphate synthesized by using boric acid flux method. *Dalton Trans.* **2011**, *40*, 2549−2554.
(26) (a) Yang, W.; Li, J.; Pan, Q.; Jin, Z.; Yu, J.; Xu, R. $Na_2[VB_3P_2O_{12}(OH)]\cdot 2.92H_2O$: A New Open-Framework Vanadium Borophosphate Containing Extra-Large 16-Ring Pore Openings and 128166 Super Cavities Synthesized by Using the Boric Acid Flux Method. *Chem.. Mater.* **2008**, *20*, 4900−4905. (b) Yang, T.; Sun, J.; Li, G.; Eriksson, L.; Zou, X.; Liao, F.; Lin, J. $Na_8[Cr_4B_{12}P_8O_{44}(OH)_4][P_2O_7]\cdot nH_2O$: A 3D Borophosphate Framework with Spherical Cages. *Chem.-Eur. J.* **2008**, *14*, 7212−7217.
(27) Hao, Y.-C.; Deng, J.; Chen, C.; Lin, Y.; Li, H.; Qin, G.; Hu, K. $Na_3[Al_2B_6P_4O_{22}(OH)_3](H_2O)_6$ and $Na_3[Al_2BP_2O_{11}](H_2O)_{0.5}$: Two Remarkable Complex Aluminum Borophosphates. *Inorg. Chem.* **2024**, *63*, 9098−9108.

https://doi.org/10.1021/acs.inorgchem.5c04481
Inorg. Chem. 2025, 64, 24754−24765

(28) (a) Wang, S.; Alekseev, E. V.; Depmeier, W.; Albrecht-Schmitt, T. E. Recent progress in actinide borate chemistry. *Chem. Commun.* **2011**, *47*, 10874−10885. (b) Silver, M. A.; Albrecht-Schmitt, T. E. Evaluation of f-element borate chemistry. *Coord. Chem. Rev.* **2016**, *323*, 36−51.
(29) (a) Lipp, C.; Burns, P. C. Th2[bo4][po4]: A Rare Example Of An Actinide Borate−phosphate. *Can. Mineral.* **2011**, *49*, 1211−1220. (b) Wu, S.; Polinski, M. J.; Malcherek, T.; Bismayer, U.; Klinkenberg, M.; Modolo, G.; Bosbach, D.; Depmeier, W.; Albrecht-Schmitt, T. E.; Alekseev, E. V. Novel fundamental building blocks and site dependent isomorphism in the first actinide borophosphates. *Inorg. Chem.* **2013**, *52*, 7881−7888. (c) Wu, S.; Wang, S.; Diwu, J.; Depmeier, W.; Malcherek, T.; Alekseev, E. V.; Albrecht-Schmitt, T. E. Complex clover cross-sectioned nanotubules exist in the structure of the first uranium borate phosphate. *Chem. Commun.* **2012**, *48*, 3479−3481.
(30) (a) Sigmon, G. E.; DiBlasi, N. A.; Hixon, A. E. The crystal chemistry of plutonium(iv) borophosphate. *Dalton Trans.* **2023**, *52*, 16601−16606. (b) Hao, Y.-C.; Murphy, G. L.; Bosbach, D.; Modolo, G.; Albrecht-Schmitt, T. E.; Alekseev, E. V. Porous Uranyl Borophosphates with Unique three dimensional Open Framework Structure. *Inorg. Chem.* **2017**, *56*, 9311−9320.
(31) (a) Ling, J.; Wu, S.; Chen, F.; Simonetti, A.; Shafer, J. T.; Albrecht Schmitt, T. E. Does Iodate Incorporate into Layered Uranyl Phosphates under Hydrothermal Conditions. *Inorg.chem.* **2009**, *48*, 10995−11001. (b) Pace, K. A.; Koch, R. J.; Smith, M. D.; Morrison, G.; Klepov, V. V.; Besmann, T. M.; Misture, S. T.; zur Loye, H. Crystal Growth of Alkali Uranyl Borates from Molten Salt Fluxes: Characterization and Ion Exchange Behavior of $A_2(UO_2)B_2O_5$ (A = Cs, Rb, K). *Inorg. Chem.* **2020**, *59*, 6449−6459. (c) Kocevski, V.; Juillerat, C. A.; Moore, E. E.; zur Loye, H.; Besmann, T. M. Understanding the Polymorphism of $A_4[(UO_2)_3(PO_4)_2O_2]$(A = Alkali Metals) Uranyl Phosphate Framework Structures. *Cryst. Growth Des.* **2019**, *19*, 966−975. (d) Juillerat, C. A.; Kocevski, V.; Besmann, T. M.; zur Loye, H. Discovery of $Cs_2(UO_2)Al_2O_5$ by Molten Flux Methods: A Uranium Aluminate Containing Solely Aluminate Tetrahedra as the Secondary Building Unit. *Inorg. Chem.* **2019**, *58*, 4099−4102.
(32) (a) *CrystalClear*, version 1.3.5; Rigaku Corp: Woodlands, TX, 1999. (b) Sheldrick, G. M. *SHELXTL, Crystallographic Software Package*,version 5.1, Bruker-AXS: Madison, WI, 1998. (c) Spek, A. L. *PLATON*; Utrecht University: Utrecht, The Netherlands, 2001.
(33) (a) Brown, I. D.; Altermatt, D. Bond-valence parameters obtained from a systematic analysis of the inorganic crystal structure database. *Acta Crystallogr., Sect. B:Struct. Sci.* **1985**, *41*, 244−247. (b) Brese, N. E.; O'Keeffe. Bond-valence parameters for solids M. *Acta Crystallogr., Sect. B:Struct. Sci.* **1991**, *B47*, 192−197.
(34) Van Acker, T.; Theiner, S.; Bolea-Fernandez, E.; Vanhaecke, F.; Koellensperger, G. Inductively coupled plasma mass spectrometry. *Nat. Rev. Methods Primers* **2023**, *3*, No. 52.
(35) Hao, Y.-C.; Murphy, Gabriel L.; Bosbach, Dirk.; Modolo, G.; Albrecht-Schmitt, T. E.; Alekseev, E. V. Porous Uranyl Borophosphates with Unique three dimensional Open Framework Structure. *Inorg. Chem.* **2017**, *56*, 9311−9320.
(36) Hao, Y.; Pan, Y.; Lin, Y.; He, L.; Ge, G.; Ruan, Y.; Zhou, H.; Xue, Y.; Koirala, K. Highly porous aluminophosphates with unique three dimensional open framework structures from mild hydrothermal syntheses. *CrystEngComm* **2020**, *22*, 3070−3078.
(37) Hao, Y.-C.; Kegler, P.; Albrecht-Schmitt, T. E.; Wang, S.; Dong, Q.; Alekseev, E. V. Two-Dimensional Uranyl Borates: From Conventional to Extreme Synthetic Conditions. *Eur. J. Inorg. Chem.* **2020**, *2020*, 407−416.
(38) (a) Shi, Y.; Pan, S.; Dong, X.; Wang, Y.; Zhang, M.; Zhang, F.; Zhou, Z. $Na_3Cd_3B(PO_4)_4$: A New Noncentrosymmetric Borophosphate with Zero-Dimensional Anion Units. *Inorg. chem.* **2012**, *51*, 10870−10875. (b) Zhang, W.; Cheng, W.; Zhang, H.; Geng, L.; Li, Y.; Lin, C.; He, Z. Syntheses and Characterizations of $Cs_2Cr_3(BP_4O_{14})(P_4O_{13})$ and CsFe(BP3O11) Compounds with Novel Borophosphate Anionic Partial Structures. *Inorg. Chem.* **2010**, *49*, 2550−2556.
(39) (a) Burns, P. C.; Kubatko, K. A.; Sigmon, G.; Fryer, B. J.; Gagnon, J. E.; Antonio, M. R.; Soderholm, L. Cover Picture: Actinyl Peroxide Nanospheres. *Angew. Chem., Int. Ed.* **2005**, *44*, 2135−2139. (b) Ling, J.; Qiu, J.; Burns, P. C. Uranyl peroxide oxalate cage and core−shell clusters containing 50 and 120 uranyl ions. *Inorg. Chem.* **2012**, *51*, 2403−2408.
(40) Qiu, J.; Burns, P. C. Clusters of actinides with oxide, peroxide, or hydroxide bridges. *Chem. Rev.* **2013**, *113*, 1097.
(41) (a) Alexandrov, E. V.; Blatov, V. A.; Kochetkov, A. V.; Proserpio, D. M. Underlying nets in three-periodic coordination polymers: topology, taxonomy and prediction from a computer-aided analysis of the Cambridge Structural Database. *CrystEngComm* **2011**, *13*, 3947−3958. (b) Blatov, V. A.; O'Keeffe, M.; Proserpio, D. M. Vertex-, face-, point-, Schläfli-, and Delaney-symbols in nets, polyhedra and tilings: recommended terminology. *CrystEngComm* **2010**, *12*, 44−48. (c) Blatov, V. A. Multipurpose crystallochemical analysis with the program package TOPOS. *IUCr CompComm Newsletter.* **2006**, *7*, No. 4.
(42) (a) Baur, W. H. On the cation and water positions in faujasite. *Am. Mineral* **1964**, *49*, 697−704. (b) Hu, J. S.; Zhong, L. S.; Song, W. G.; Wan, L. J. Synthesis of hierarchically structured metal oxides and their application in heavy metal ion removal. *Adv. Mater.* **2008**, *20*, 2977−2982. (c) Fu, F.; Wang, Q. J. Removal of heavy metal ions from wastewaters: a review environ. *Management* **2011**, *92*, 407−418. (d) Manos, M. J.; Chrissafis, K.; Kanatzidis, M. G. Unique Pore Selectivity for Cs^+ and Exceptionally High NH^{4+} Exchange Capacity of the Chalcogenide Material $K_6Sn[Zn_4Sn_4S_{17}]$. *J. Am. Chem. Soc.* **2006**, *128*, 8875−8883. (e) Manos, M. J.; Kanatzidis, M. G. Highly Efficient and Rapid Cs+ Uptake by the Layered Metal Sulfide K2xMnxSn3−xS6 (KMS-1). *J. Am. Chem. Soc.* **2009**, *131*, 6599−6607.
(43) Katada, N.; Tamura, H.; Matsuda, T.; Kawatani, Y.; Moriwaki, Y.; Matsuo, M.; Kato, R. Correlation between Na−Cs Ion Exchange Properties in the Alkaline Form and Acid Strength in the Proton Form of Zeolite. *J. Am. Chem. Soc.* **2024**, *40*, 19324−19331.
(44) Ouyang, Z.; Li, X.; Zhang, J.; Li, B.; Long, H.; Zhang, Y.; Yu, K.; Li, Y.; Ma, L. Zwitterionic adsorbents derived from self-Exfoliated ionic covalent organic frameworks for efficient Co-Removal of anionic and cationic radionuclides. *Chem. Eng. J.* **2024**, *497*, No. 154882.
(45) Zhang, M.; Qin, Y.; Zhang, F.; Feng, Y.; Ozer, S. N.; Sun, W.; Zhao, Y.; Xu, Z. Site-selective etching and conversion of bismuth-based Metal−Organic frameworks by oxyanions enables efficient and selective adsorption via robust coordination bonding[J]. *Chem. Eng. J.* **2024**, *488*, No. 150867.
(46) (a) Mertz, J. L.; Fard, Z. H.; Malliakas, C. D.; Manos, M. J.; Kanatzidis, M. G. Selective Removal of Cs^+, Sr^{2+}, and Ni^{2+} by $K_{2x}Mg_xSn_3-xS_6$ (x = 0.5−1) (KMS-2) Relevant to Nuclear Waste Remediation. *Chem. Mater.* **2013**, *25*, 2116−2127. (b) Sarma, D.; Malliakas, C. D.; Subrahmanyam, K. S.; Islam, S. M.; Kanatzidis, M. G. K2xSn4−xS8−x(x = 0.65−1): a new metal sulfide for rapid and selective removal of Cs+, Sr2+and UO22+ions. *Chem. Sci.* **2016**, *7*, 1121−1132.
(47) Feng, M.-L.; Sarma, D.; Gao, Y.-J.; Qi, X.-H.; Li, W.-A.; Huang, X.-Y.; Kanatzidis, M. G. Efficient removal of $[UO_2]^{2+}$, Cs^+, and Sr^{2+} ions by radiation-resistant gallium thioantimonates. *J. Am. Chem. Soc.* **2018**, *140*, 11133−11140.
(48) Wu, Z.; Weigend, F.; Fenske, D.; Naumann, T.; Gottfried, J. M.; Dehnen, S. Ion-Selective Assembly of Supertetrahedral Selenido Germanate Clusters for Alkali Metal Ion Capture and Separation. *J. Am. Chem. Soc.* **2023**, *145* (6), 3802−3811.
(49) Wang, C.-C.; Chang, C.-Y.; Chen, C.-Y. Study on metal ion adsorption of bifunctional chelating/ion-exchange resins. *Macromol. Chem. Phys.* **2001**, *202*, 882−890.
(50) (a) U. S. Food and Drug Administration. 2015; Vol. *41*. (b) Amor, Z.; Bariou, B.; Mameri, N.; Taky, M.; Nicolas, S.; Elmidaoui, A. Fluoride removal from brackish water by electrodialysis. *Desalination* **2001**, *133*, 215−223. (c) Matlock, M. M.; Howerton, B. S.; Atwood, D. A. Chemical precipitation of heavy metals from acid mine drainage. *Water Res.* **2002**, *36*, 4757−4767. (d) Keskinkan, O.; Goksu, M. Z. L.; Basibuyuk, M.; Forster, C. F. Heavy metal

https://doi.org/10.1021/acs.inorgchem.5c04481
Inorg. Chem. 2025, 64, 24754−24765

adsorption properties of a submerged aquatic plant (Ceratophyllum demersum). *Bioresour. Technol.* **2004**, *92*, 197−200. (e) Dai, S.; Ju, Y. H.; Barnes, C. E. Solvent extraction of strontium nitrate by a crown ether using room-temperature ionic liquids. *Dalton Trans.* **1999**, *8*, 1201−200. (f) Ahmed, S.; Chughtai, S.; Keane, M. A. The removal of cadmium and lead from aqueous solution by ion exchange with NaY zeolite. *Sep. Purif. Technol.* **1998**, *13*, 57−64. (g) Ćurković, L.; Cerjan-Stefanović, Š.; Filipan, T. Metal ion exchange by natural and modified zeolites. *Water Res.* **1997**, *31*, 1379−1382.

(51) (a) Grinstead, R. R. Selective absorption of copper, nickel, cobalt and other transition metal ions from sulfuric acid solutions with the chelating ion exchange resin XFS 4195. *Hydrometallurgy* **1984**, *12*, 387−400. (b) Zhao, X.; Bu, X.; Wu, T.; Zheng, S. T.; Wang, L.; Feng, P. Selective anion exchange with nanogated isoreticular positive metal-organic frameworks. *Nat. Commun.* **2013**, *4*, No. 1. (c) Qiu, W.; Zheng, Y. Removal of lead, copper, nickel, cobalt, and zinc from water by a cancrinite-type zeolite synthesized from fly ash. *Chem. Eng. J.* **2009**, *145*, 483−488. (d) Deák, A.; Tunyogi, T.; Pálinkás, G. Synthesis and structure of a cyanoaurate-based organotin polymer exhibiting unusual ion-exchange properties. *J. Am. Chem. Soc.* **2009**, *131*, 2815−2817.

(52) Park, K. C.; Martin, C. R.; Leith, G. A.; Thaggard, G. C.; Wilson, G. R.; et al. Capture Instead of Release: Defect-Modulated Radionuclide Leaching Kinetics in Metal−Organic Frameworks. *J. Am. Chem. Soc.* **2022**, *144*, 16139−16149.

(53) Mu, L.; Hou, D.; Foley, E. E.; Dai, M.; Zhang, J.; Jiang, Z.; Rahman, M. M.; Fu, Y.; Ma, L.; Hu, E.; Sainio, S.; Nordlund, D.; Liu, J.; Hu, J.-M.; Liu, Y.; Clément, R. J.; Lin, F. Revealing the Chemical and Structural Complexity of Electrochemical Ion Exchange in Layered Oxide Material. *J. Am. Chem. Soc.* **2024**, *146*, 26916−26925.

(54) Watanabe, S.; Hiraide, S.; Arima, H.; Fukuta, A.; Mori, M.; Tanaka, H.; Miyahara, M. T. Size-dependent guest-memory switching of the flexible and robust adsorption characteristics of layered metal-organic frameworks. *Sci. Adv.* **2024**, *10*, No. eadr1387.

(55) Lu, P.; Xu, J.; Sun, Y.; Guillet-Nicolas, R.; Willhammar, T.; Fahda, M.; Dib, E.; Wang, B.; Qin, Z.; Xu, H.; Cho, J.; Liu, Z.; Yu, H.; Yang, X.; Lang, Q.; Mintova, S.; Zou, X.; Valtchev, V. A stable zeolite with atomically ordered and interconnected mesopore channel. *Nature* **2024**, *636*, 368−373.

(56) Zhou, J.; Liu, H.; Wang, S.; Yuan, L.; Dridi, N.; Wang, S.; Mattoussi, H.; Li, X. Ca^{2+} induced highly fluorescent CsPb $(Br/Cl)_3$ perovskite quantum dots via fast Anion-Exchange & Cation-Doping Inter-Promotion strategy for efficient deep-blue light-emitting diodes. *Chem. Eng. J.* **2024**, *489*, No. 151227.

(57) Hao, Y.-C.; Zhang, Y.; Zhang, Y.-Y.; Fu, Z.-X.; Heng, C.-Y.; Li, J.-J.; You, J.-T.; Hu, K.-H.; Lin, Y.; Li, H.-J. A series of novel phosphites/phosphates with deep-ultraviolet cut-off edges. *CrystEngComm* **2023**, *25* (34), 4864−4872.

(58) Li, X.; Zhang, Y.; Pan, Y.; Hao, Y.; Lin, Y.; Li, H.; Li, M.; Fan, C.; Alekseev, E. V. $Li_3[Al(PO_4)_2(H_2O)_{1.5}]$ and $Na[AlP_2O_7]$: from 2D layered polar to 3D centrosymmetric framework structures. *CrystEngComm* **2022**, *24*, 6917−6924.

(59) Yu, Y.; Hao, Y.-C.; Xiao, B.; Langer, E.; Novikov, S. A.; Ramanantoanina, H.; Pidchenko, I.; Schild, D.; Albrecht-Schoenzart, T. E.; Eichel, R. -A.; Vitova, T.; Alekseev, E. V. U(V) Stabilization via Aliovalent Incorporation of Ln(III) into Oxo-salt Framework. *Chem.-Eur. J.* **2024**, *30*, No. e202401033.

(60) Hao, Y.-C.; Langer, E. M.; Xiao, B.; Kegler, P.; Cao, X.; Hu, K.; Eichel, R.-A.; Wang, S.; Alekseev, E. V. Understanding of the structural chemistry in the uranium oxo-tellurium system under HT/HP conditions. *Front. Chem.* **2023**, *11*, No. 1152113.

(61) Hao, Y.-C.; Klepov, V. V.; Kegler, P.; Modolo, G.; Bosbach, D.; Albrecht-Schmitt, T. E.; Wang, S.; Alekseev, E. V. Synthesis and Study of the First Zeolitic Uranium Borate. *Cryst. Growth Des.* **2018**, *18*, 498−505.

(62) (a) Hao, Y.-C.; Klepov, V. V.; Murphy, G. L.; Modolo, G.; Bosbach, D.; Albrecht-Schmitt, T. E.; Kennedy, B. J.; Wang, S.; Alekseev, E. V. Influence of synthetic conditions on chemistry and structural properties of alkaline earth uranyl borates. *Cryst. Growth Des.* **2016**, *16*, No. 5923. (b) Shi, Y.; Liang, J.; Zhang, H.; Liu, Q.; Chen, X.; Yang, J.; Zhuang, W.; Rao, G. Crystal structure and thermal decomposition studies of barium borophosphate, $BaBPO_5$ Solid State. *J. Chem.* **1998**, *135*, 43−51.

https://doi.org/10.1021/acs.inorgchem.5c04481
Inorg. Chem. 2025, 64, 24754−24765